Spectral homogenization techniques for the Hyperspectral Image Projector

Logan E. Hillberry[1] and Joseph P. Rice[2]

[1]Dept. of Physics, 1523 Illinois Street, Colorado School of Mines Golden, CO 80401
[2]National Institute of Standards and Technology, Gaithersburg, MD 20899

ABSTRACT

In an effort to improve technology for performance testing and calibration of multispectral and hyperspectral imagers, the National Institute of Standards and Technology (NIST) has been developing a Hyperspectral Image Projector (HIP) capable of projecting dynamic scenes than include distinct, programmable spectra in each of its 1024 × 768 spatial pixels. The HIP is comprised of a spectral engine, which is a light source capable generating the spectra in the scene, coupled to a spatial engine, capable of projecting the spectra into the correct locations of the scene. In the prototype HIP, the light exiting the Visible-Near-Infrared (VNIR) / Short-Wavelength Infrared (SWIR) spectral engine is spectrally dispersed and needs to be spectrally homogenized before it enters the spatial engine. In this paper we describe the results from a study of several different techniques for performing this spectral homogenization. These techniques include an integrating sphere, a liquid light guide, a randomized fiber bundle, and an engineered diffuser, in various combinations. The spectral uniformity of projected HIP scenes is measured and analyzed using the spectral angle mapper (SAM) algorithm over the VNIR spectral range. The SAM provides a way to analyze the spectral uniformity independently from the radiometric uniformity. The goal of the homogenizer is a spectrally uniform and bright projected image. An integrating sphere provides the most spectrally uniform image, but at a great loss of light compared with the other methods. The randomized fiber bundle generally outperforms the liquid light guide in both spectral homogenization and brightness. Using an engineered diffuser with the randomized fiber bundle increases the spectral uniformity by a factor of five, with a decrease in brightness by a factor of five, compared with the randomized fiber bundle alone. The combination of an engineered diffuser with a randomized fiber bundle provides comparable spectral uniformity to the integrating sphere while enabling 40 times greater brightness.

Keywords: diffuser, fiber bundle, hardware-in-the-loop, hyperspectral, imaging, scene projector, spectral uniformity

1. INTRODUCTION

For the past several years NIST has been developing, along with several collaborators, a Hyperspectral Image Projector (HIP) [1-12]. This scene projector produces high-resolution programmable spectra and projects them into dynamic two-dimensional images. The current digital micromirror device (DMD) based HIP prototype has a spatial resolution of 1024 x 768 pixels and a spectral range of 450 nm to 2400 nm, with spectral resolution from 2 nm in the visible to 5 nm in the short-wave infrared. It disperses light from a supercontinuum fiber source across two DMDs (one in the visible-near-infrared (VNIR) and another in the short-wavelength infrared (SWIR)) in the spectral engine, then re-combines them to produce programmable spectra, which then globally-illuminate a third DMD in the spatial engine to form the spatial images that are collimated for viewing by the unit under test (UUT). In addition to the VNIR-SWIR HIP, a mid-wavelength infrared (MWIR) HIP and an ultraviolet-visible (UVis) HIP extension are currently being constructed.

A challenging technical problem in the spectral engine design has been finding the optimal method of re-combing the dispersed spectra to provide spectral-spatial homogeneous illumination of the spatial engine. That is, it is desired that for a spatially uniform scene, the spectrum of light illuminating any given pixel of the spatial engine DMD is identical to all the others. Note that this problem is related to the traditional radiometric non-uniformity problem in conventional hardware-in-the-loop projectors, but can be thought of as separate: we can obtain relative spectral-spatial homogeneity (so that the shapes of the spectra are uniform) but still have conventional radiometric non-uniformity across the scene if the absolute radiance levels vary. This paper addresses this spectral uniformity issue, rather than the traditional radiometric uniformity. Once spectral uniformity is achieved, radiometric uniformity will be addressed separately by using the gray scale of the spatial engine DMD.

In the breadboard HIP that we described previously, the spectral-spatial homogeneity was obtained by using a prism after the DMD to spatially recombine the dispersed spectrum. The spectral engine can be thought of as a double subtractive spectrograph with a DMD at an intermediate image plane. For a symmetric layout, the spectral-spatial recombination could in principle be exact. However, the DMD breaks the symmetry in two ways. The first is that the image plane after the spectral engine DMD is tilted because of the tilt of the individual DMD mirrors. The second is that DMD diffraction causes additional spectral-spatial non-uniformity, including the separation of diffraction orders over a broad spectral range [6]. These issues were overcome in the breadboard version of the HIP, which covered the visible-band only, by adding an integrating sphere after the recombining prism [3]. This provides the required homogenization, but at the expense of great loss of light since integrating spheres do not provide high transmittance. To achieve our goal of matching top-of-the atmosphere radiance levels over the very broad spectral range of the VNIR-SWIR prototype HIP, we sought a higher throughput technology than integrating spheres. That motivated the study reported in this paper.

2. COUPLING/HOMOGENIZATION METHODS

For practical reasons, it is desirable for the spectral engine and spatial engines in the HIP prototype to be separated by a couple of meters in the lab, connected by a flexible light-transmitting coupling. This enables the spatial engine to be on a translation stage to facilitate alignment to the UUT and calibration against a reference instrument, while the spectral engine is stationary in an equipment rack. One coupling option is a commercially-available (Newport* Model 77639) Liquid Light Guide (LLG). The LLG consists of a fluid-filled flexible light-transmitting tube that has a nominal internal diameter of 8 mm and a nominal length of 2 m, and a numerical aperture of 0.52. It operates via total internal reflection, so through multiple reflections down the guide there is some spectral-spatial mixing by the time the light exits the LLG at the spatial engine. This method has shown to be radiometrically efficient (that is, it allows for the bright projection of scenes) but residual spectral non-uniformity is evident, as will be quantified below. The transmittance bandwidth of the LLG is from 420 nm to 2000 nm, so it unfortunately truncates the SWIR output of the spectral engine from 2000 nm to 2400 nm.

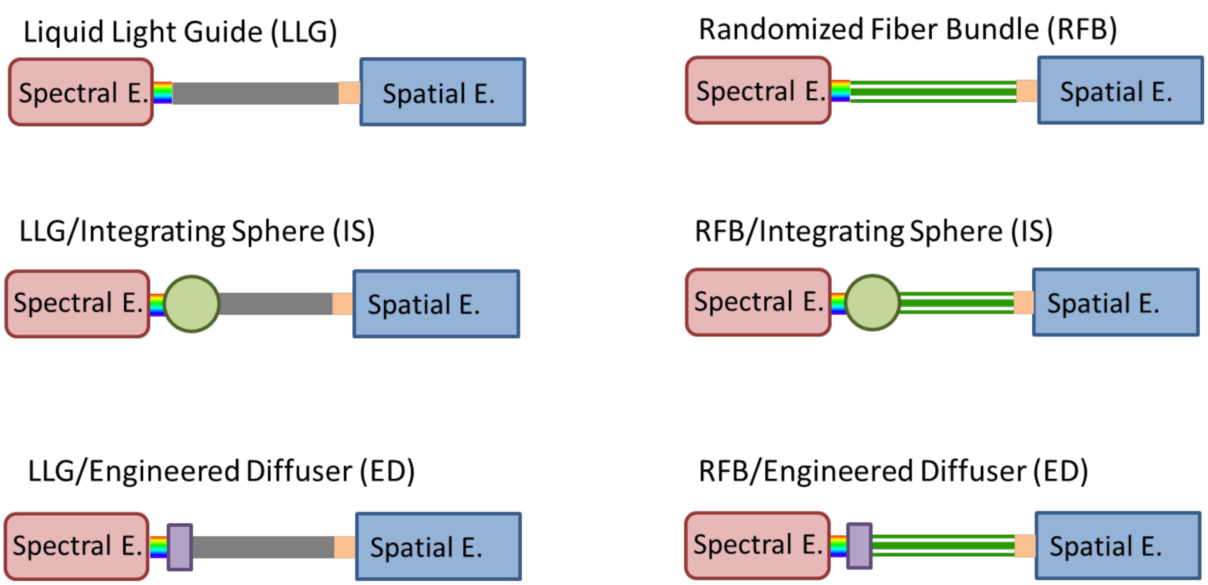

Figure 1. Coupling/homogenization methods between the HIP Spectral Engine (Spectral E.) and the HIP Spatial Engine (Spatial E.) considered in this study.

As an alternative, we investigated a custom-made (CeramOptec) randomized fiber bundle (RFB) as a coupling/homogenization method. In this device, 874 closely-packed infrared grade fused-silica fibers (200 micrometer core diameter, 220 micrometer cladding diameter, 245 micrometer nominal sheath diameter, a numerical aperture of 0.22, OH content less than 0.25 µg/g) are used as dielectric waveguides, but the output configuration of fibers is randomized relative to the input. The RFB is covered with a protective metal sheath, has a nominal length of 2 m, and a ferrule design enabling it to swap with the LLG. At each end the individual silica fibers are fused to reduce the non-uniformity resulting from the individual fiber cladding. Two RFBs of the same specifications were produced and tested.

Either the LLG or RFB provides the coupling between the spectral and spatial engine. However, we also investigated additional homogenization methods to increase the spectral uniformity of the projected data cube while tracking the loss of brightness ensued by these add-ons. One option is to place an integrating sphere (IS) between the spectral engine and the LLG or RFB. The commercially-available (Thorlabs Model IS236A-4) IS that we used is a hollow block of high diffuse-reflectance polytetrafluoroethylene having a spherically-shaped internal wall about 50 mm in diameter and small ports for the input beam, output beam, and a silicon photodiode monitor. The entrance port accepts light directly from the spectral engine and the exit port is situated orthogonal to the entrance port. With such geometry, the entering light must reflect multiple times until it reaches the exit. This effectively homogenizes the light, but at a great cost of radiometric power. The other option that we tested was to replace the integrating sphere with a commercially-available (RPC Photonics Model ED1-C20) engineered diffuser (ED). For a normal incidence collimated beam, this diffuser provides a homogeneous circular output beam having 20 degree divergence. Inserted between the output of the spectral engine and the input of the LLG or RFB, this ED provides homogenization with greater transmittance than the IS, as we demonstrate below.

In total, there are six coupling/homogenization methods that we tested, as depicted in Fig. 1. The LLG alone, LLG/IS, and the LLG/ED. Analogously, there is the RFB alone, RFB/IS, and RFB/ED.

3. QUANTIFYING THE SPECTRAL UNIFORMITY AND BRIGHTNESS

Here, we describe the methods and metrics to quantitatively compare the six coupling/homogenizing methods. Each configuration is subject to the same tests and analysis.

3.1. Tests

To test the spectral uniformity of a given configuration, we scanned through a set of monochromatic bands on the spectral engine with the spatial engine set to display a uniform scene. We recorded the image projected by the HIP at each band using an unfiltered charge-coupled device (CCD) camera (Fig. 2a). The HIP collimator lens (focal length, f = 100 mm) and the camera lens (f = 85 mm) were focused at infinity so that the image projected by the spatial engine DMD was focused onto the CCD as in Ref. 2, and the camera lens had a variable aperture stop that allowed for different relative aperture settings (*f*/#'s). For each configuration, a VNIR data cube was projected by turning all spatial engine DMD mirrors on and scanning columns of the spectral engine DMD mirrors. More precisely, the spectrum was divided into 96 bands, each about 6 nm wide (corresponding to about 10 spectral engine DMD columns), covering a spectral range of 450 nm to 1020 nm. The light of each band was guided to the spatial engine via the coupling configuration-under-test, and the CCD camera recorded the image from each band individually during a 0.1 second exposure time. Interposed with these monochromatic spectral engine frames were dark frames where all spectral engine DMD mirrors were off. We corrected for stray light by subtracting the dark frames from the monochromatic frames, and built up the data cube by assembling the dark-corrected frames captured from each of the 96 monochromatic bands. We measured a data cube in this way for each of the six coupling/homogenization configurations and at several different *f*/#'s on the CCD camera lens. The *f*/#'s on the camera lens included *f*/2, *f*/2.8, and *f*/4. Varying the *f*/# ensures the conclusions we draw about the configurations hold for a variety of aperture sizes of the UUT.

To test the relative brightness of a given configuration, we replaced the CCD with a spectroradiometer coupled via a 100 mm diameter integrating sphere (Fig. 2b). We used the same camera lens, set to the same *f*/# and positioned in the same location, for both the CCD measurements and the spectroradiometer measurements. For the spectroradiometer measurements, the lens focused the spatial engine DMD image at the entrance port of the integrating sphere. The image under-filled the entrance port. Both the VNIR spectral engine and the spatial engine DMDs were set to all-mirrors on, and the spectroradiometer measured the spectrum. A spectrum was recorded for each of the three *f*/#s and the six coupling/ homogenization configurations. The spectroradiometer data do not directly represent the absolute spectral radiance delivered to the UUT, because for that the (unknown) transmittance of the integrating sphere between the spatial engine and the spectroradiometer would need to be factored out. However, in the next section we describe how these spectra were used to measure relative differences in radiance between different configurations.

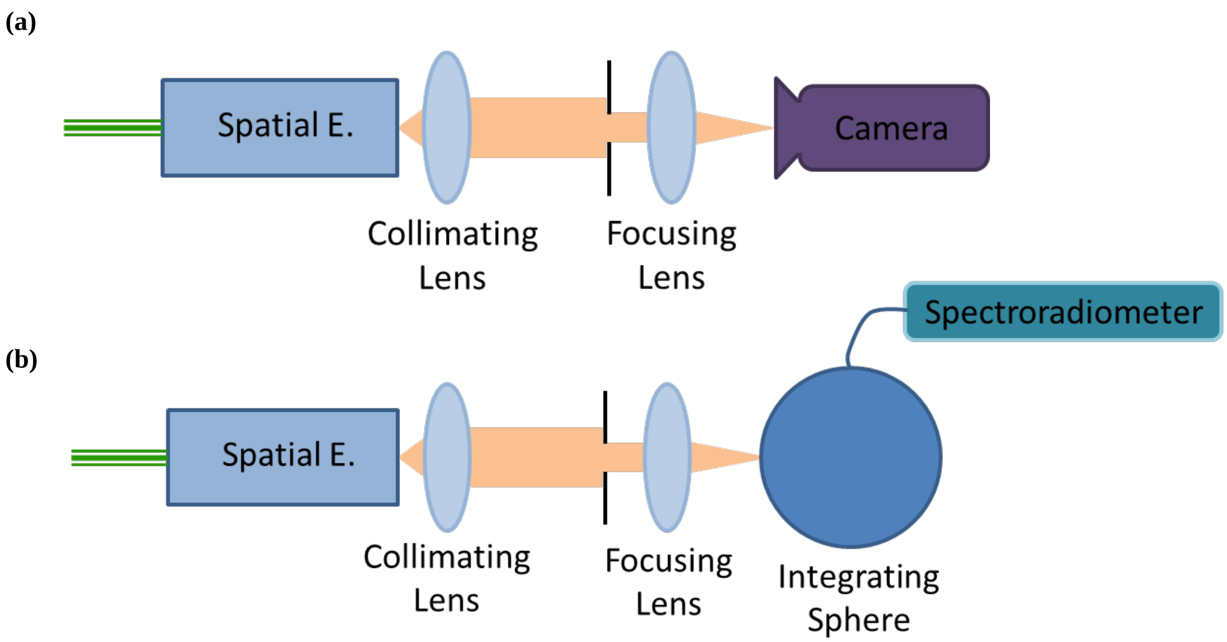

Figure 2. Hardware configuration used to measure (a) spectral uniformity and (b) relative brightness.

3.2. Analysis

The data cubes collected by the CCD camera were used to check the spectral uniformity (i.e., the similarity between two spatially distinct pixels that ideally have the same spectrum) of a given coupling/homogenization configuration. To do this, we make use of the spectral angle mapper (SAM) routine in the hyperspectral data analysis software called Environment for Visualizing Images (ENVI, Exelis Visual Information Solutions). Spectral angle is a metric which measures the similarity between two spectra independent of radiometric variations [13]. The concept can be visualized as in Fig. 3 for three bands. Any spectrum can plotted as a single point where the coordinates of the point are given by the value of the spectrum in each band. Though it cannot be visualized, the concept generalizes to N bands, such as our case of 96 bands, where any spectrum still plots as a single point in N-dimensional space. Any spectrum can then be thought of as vector from the origin to the point, and the spectral angle is the angle between any two such vectors. The spectral angle θ_{ij} between the spectrum $\boldsymbol{s}_{ij}$, from pixel (i, j) of the data cube, and a reference spectrum, $\boldsymbol{r}$, may be calculated as

$$\theta_{ij} = \cos^{-1}\left(\frac{\boldsymbol{s}_{ij} \bullet \boldsymbol{r}}{\left|\boldsymbol{s}_{ij}\right|\left|\boldsymbol{r}\right|}\right). \quad (1)$$

The spectral angle is small between any two spectra having similar features, and it grows as the two spectra become more distinct. We used SAM to calculate the spectral angle between each pixel and the average spectrum of the entire image. That is, for each data cube we measured as described in Section 3.1, we first found the average spectrum of all the pixels and set that to the reference spectrum $\boldsymbol{r}$. Then θ_{ij} was calculated, using Eq. (1), for the spectrum $\boldsymbol{s}_{ij}$ of each pixel (i, j) and stored in an array. This array can be visualized either as a map (low spectral angles are more black and high spectral angles are more white), which is called as a "rule image" in ENVI, or as a histogram of the number of pixels with a given spectral angle. The rule image gives a qualitative picture of the spectral uniformity because, ideally, the spectra of all pixels are identical which would give a black rule image. In reality, since each pixel will not have the same spectrum, the spectral uniformity of the image must measure how much the spectrum of each pixel deviates from the average. To this end, we define our metric for spectral uniformity to be the standard deviation, $\sigma(\theta_{ij})$, of the spectral angles calculated by SAM. A small $\sigma(\theta_{ij})$ means a more spectrally uniform scene. We computed $\sigma(\theta_{ij})$ from the histograms of SAM maps from the data cubes for each of the six configurations in Fig. 1 and each of the three *f*/#s measured as described in Section 3.1.

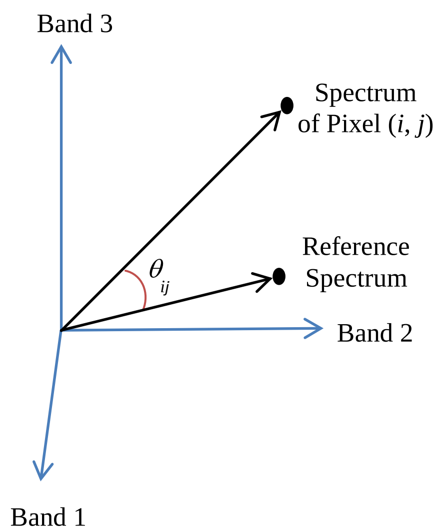

Figure 3. The concept of spectral angle θ_{ij} for three bands, which form a set of orthogonal basis vectors that span an abstract space. Any spectrum is plotted as a single point where the coordinates of the point are given by the value of the spectrum in each band. The concept generalizes to N bands, and the spectrum from each pixel of the data cube has a unique spectral angle relative to a reference spectrum.

The spectral radiance data collected by the spectroradiometer was used to compare relative brightness of the different coupling/homogenization options. While the spectrum itself contains more information as to which particular wavelength is brighter (higher spectral radiance), we desire a single number to characterize the brightness of each configuration. Our brightness metric is thus defined as radiance, computed simply as the wavelength integral of spectral radiance. We computed relative radiance from the spectroradiometer data for each of the six configurations and each of the three *f*/#s.

4. RESULTS

The results of the spectral uniformity analysis are displayed in Fig. 4. Recall that two different RFBs (RFB#1 and RFB#2) were tested without any additional homogenizing elements. The RFB's showed improved spectral uniformity (smaller standard deviation of spectral angle) over a larger aperture (*f*/#) compared with the LLG. The configurations with the additional homogenizing elements (RFB/IS and RFB/ED, performed with RFB#1 only) were consistently much more uniform than those without these elements.

The standard uncertainty of the spectral angle standard deviation measurements, indicated by the error bar in Fig. 4, includes repeatability and noise from the individual measurements of $\sigma(\theta_{ij})$, and systematic effects from using the standard deviation as a metric to quantify the histograms of spectral angle for each image.

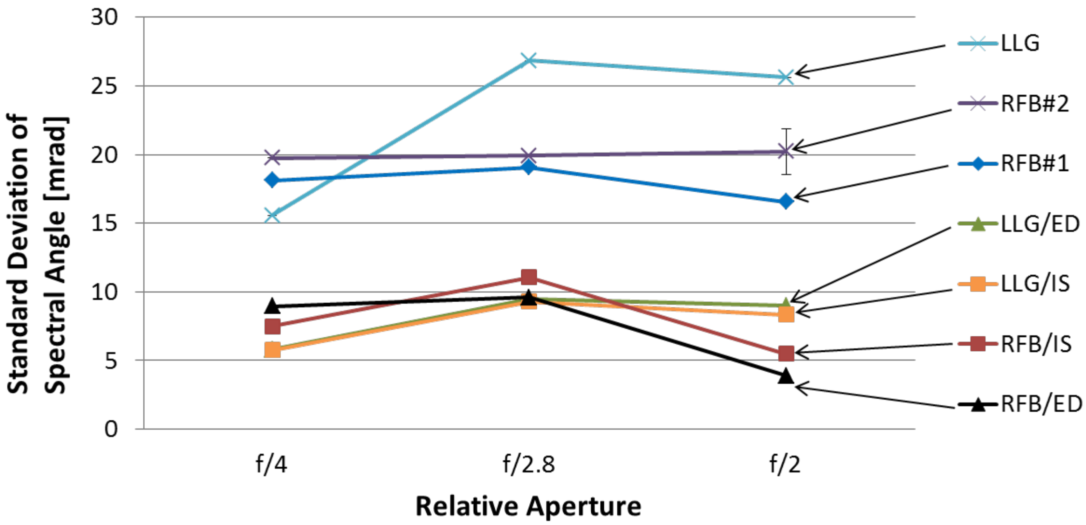

Figure 4. Results from the spectral angle analysis of the different coupling/homogenization methods. The error bar shown on the RFB#2 *f*/2 result represents the standard uncertainty of $\sigma(\theta_{ij})$, and is similar for all the results but not plotted to maintain clarity.

In Fig. 5 we show the results of the relative radiance measurements. To define relative radiance, the values of radiance have for each *f*/# have been normalized to that of RBF#2 for that *f*/#. Again, similar configurations tend to cluster together, though the overall range of radiance spans more than two orders of magnitude. The configuration with the least amount of light loss is the RFB alone (RFB#1 and RFB#2 lie on top of each other in this plot), closely followed by the LLG alone. The most loss was caused by adding an integrating sphere, as we expected. The standard uncertainty of each of the relative radiance measurements is estimated to 0.1 % of the value, based upon the standard deviation of three repeated measurements.

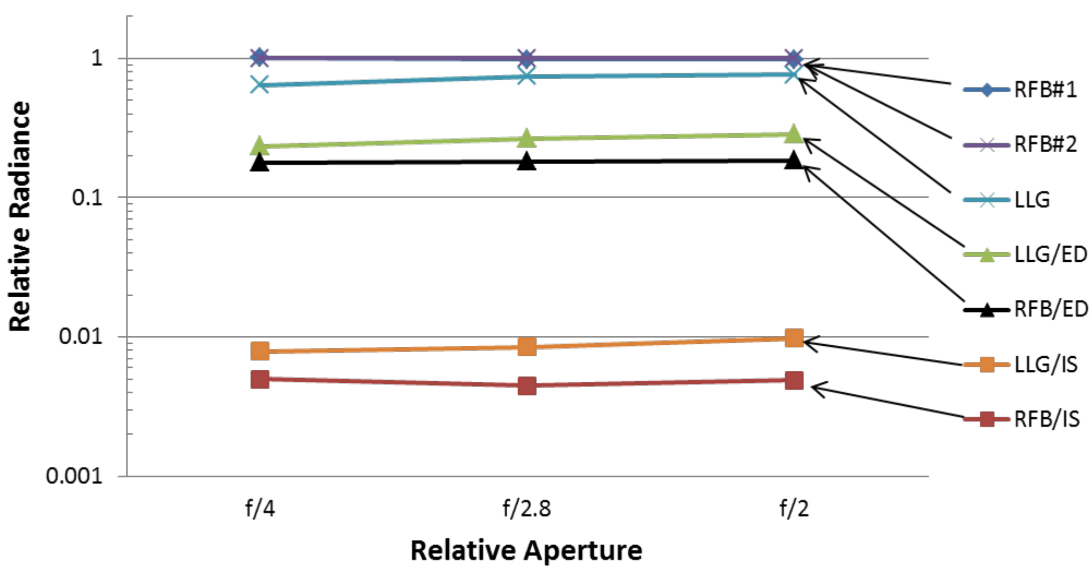

Figure 5. Results from the radiance measurements of the different coupling/homogenization methods.

We plot radiance vs standard deviation of spectral angle for the *f*/2 data set in Fig. 6. This plot allows one to easily estimate the loss in brightness for the improvement in spectral uniformity caused by a given coupling/homogenization method. The RFB/ED combination gives the highest spectral uniformity with only a factor of five lower radiance than the RFB alone. Similar plots can be constructed for the *f*/2.8 and *f*/4 data sets, but the conclusion is the same: Optimal coupling/homogenization is obtained with the combination of the randomized fiber bundle and the engineered diffuser.

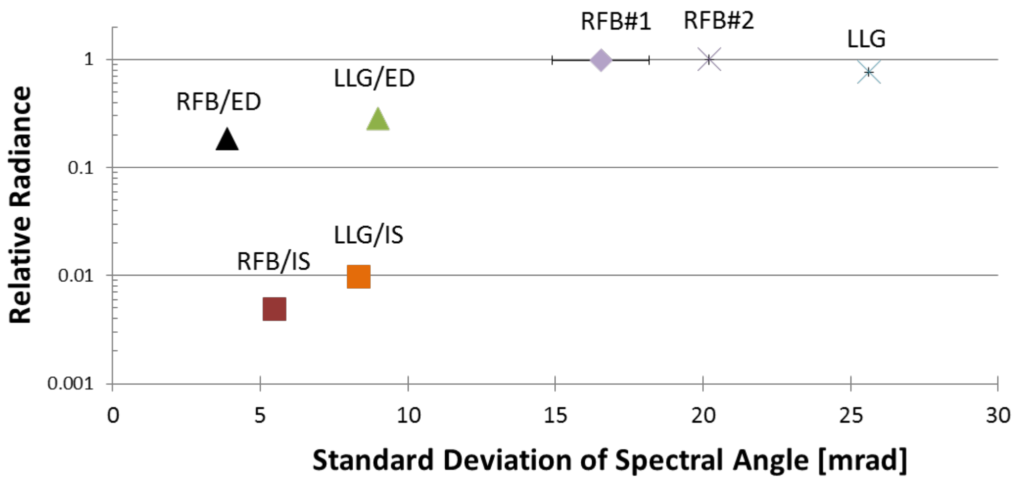

Figure 6. Radiance vs. spectral uniformity for *f*/2. The error bar shown on the RFB#1 result represents the standard uncertainty of $\sigma(\theta_{ij})$, and is similar for all the results but not plotted to maintain clarity.

A visual example of the difference between using the LLG and the RFB/ED is shown in Fig. 7. These are red-green-blue (RGB) images made from three bands of the projected HIP data cubes for the respective coupling configurations. Fig. 7a displays spectral non-uniformity in what is supposed to be a spectrally uniform scene. Fig. 7b shows the improvement in spectral uniformity made by using the RRF/ED while showing residual radiometric non-uniformity. In principle this residual radiometric non-uniformity can be corrected using the grey scale of the individual spatial engine DMD pixels, which will be the subject of a future study.

(a)

(b)

Figure 7. RGB images of the projected HIP images for (a) LLG coupling and (b) RFB/ED coupling.

5. SUMMARY

Several methods for coupling the HIP spectral engine to the HIP spatial engine were tested. This coupling also serves as a spectral homogenizer of the spectral engine light, so ideally, it provides spectrally well-mixed light to the spatial engine DMD at a minimal loss of radiance. To test several coupling/homogenization options, we developed two distinct metrics. The spectral uniformity of a given configuration is calculated as the standard deviation of the spectral angle between each pixel and the average spectrum of a data cube. The brightness of a given configuration is calculated as the relative radiance of the scene delivered by the spatial engine. Using these metrics, we produced Fig. 6 which compares the spectral uniformity to the relative radiance for each of the six configurations for a UUT aperture of *f*/2. From this plot, we conclude that the RFB out performs the LLG both alone and with the addition of either the IS or the ED. Compared with the RBF alone, the RFB/ED increases spectral uniformity by a factor of about 5 for a decrease in brightness by a factor of 5. The RFB/IS increases spectral uniformity by a factor of about 3 over the RFB alone, but with a decrease in brightness by a factor of about 200. Thus the combination of an engineered diffuser with a randomized fiber bundle provides comparable spectral uniformity to the integrating sphere while enabling 40 times greater brightness.

*Note: References are made to certain commercially available products in this paper to adequately specify the experimental procedures involved. Such identification does not imply recommendation or endorsement by the National Institute of Standards and Technology, nor does it imply that these products are the best for the purpose specified.

ACKNOWLEDGEMENTS

We thank Dr. David Allen of NIST for suggesting the randomized fiber bundle concept. L. E. Hillberry performed this work as a part of a 2014 NIST Summer Undergraduate Research Fellowship supported in part by the National Science Foundation under Grant No. PHY-1004975 and in part by the NIST Physical Measurement Laboratory.

REFERENCES

[1] Rice, J. P., Brown, S. W., Allen, D. W., Yoon, H. W., Litorja, M., and Hwang, J. C., "Hyperspectral image projector applications," *Proc. SPIE* **8254**, 82540R-1 (2012).

[2] Rice, J. P., "Analytic determination of optimal projector lens design requirements for pixilated projectors used to test pixilated imaging sensors," *Proc. SPIE* **8707**, 870702-1 (2013).

[3] Rice, J. P., Allen, D. W., "Hyperspectral image compressive projection algorithm," *Proc. SPIE* **7334**, 733414 (2009).

[4] Allen, D. W., Rice, J. P., and Goodman, J. A., "Hyperspectral projection of a coral reef scene using the NIST hyperspectral image projector," *Proc. SPIE* **7334**, 733415 (2009).

[5] Rice, J. P., Brown, S. W., Neira, J. E., and Bousquet, R. R., "A hyperspectral image projector for hyperspectral imagers," *Proc. SPIE* **6565**, 65650C (2007).

[6] Rice, J. P., Neira, J. E., Kehoe, M., and Swanson, R., "DMD diffraction measurements to support design of projectors for test and evaluation of multispectral and hyperspectral imaging sensors," *Proc. SPIE* **7210**, 72100D (2009).

[7] Brown, S. W., Myers, B., Barnes, R. A., and Rice, J. P., "Characterization of Earth observing satellite instruments for response to spectrally and spatially variable scenes," *Proc. SPIE* **6677**, 667705 (2007).

[8] Rice, J. P., Brown, S. W., and Neira, J. E., "Development of hyperspectral image projectors," *Proc. SPIE* **6297**, 629701 (2006).

[9] Brown, S. W., Rice, J. P., Neira, J. E., and Johnson, B. C., "Hyperspectral image projector for advanced sensor characterization," *Proc. SPIE* **6296**, 629602 (2006).

[10] Brown, S. W., Rice, J. P., Allen, D. W., Zuzak, K., Livingston, E., and Litorja, M., "Dynamically programmable digital tissue phantoms," *Proc. SPIE* **6870**, 687003 (2008).

[11] Brown, S. W., Rice, J. P., Neira, J. E., Johnson, B. C., and Jackson, J. D., "Spectrally tunable sources for advanced radiometric applications," *J. Res. Natl. Inst. Stand. Technol.* **111**, 401-410 (2006).

[12] Rice, J. P., Brown, S. W., Johnson, B. C., and Neira, J. E., "Hyperspectral image projectors for radiometric applications," *Metrologia* **43**, S61-S65 (2006).

[13] Schott, J. R., [Remote sensing: the image chain approach, 2nd Edition], Oxford University Press, Oxford & New York, 433 (2007).